

Possible hadronic origin of TeV photon emission from SNR G106.3+2.7

Chuyuan, Yang¹, Houdun, Zeng^{2,3}, Biwen, Bao^{3,4}, and Li, Zhang³

¹ Yunnan Observatories, Chinese Academy of Sciences, Kunming 650011, China

² Key Laboratory of Dark Matter and Space Astronomy, Purple Mountain Observatory, Chinese Academy of Sciences, Nanjing 210034, China

³ Department of Astronomy, Key Laboratory of Astroparticle Physics of Yunnan Province, Yunnan University, Kunming 650091, China

⁴ Key Laboratory of Statistical Modeling and Data Analysis of Yunnan Province, Yunnan University, Kunming 650091, China
e-mail: lizhang@ynu.edu.cn

Received ; accepted

ABSTRACT

Context. Recently, HAWC, AS γ , and LHAASO experiments have reported the gamma-ray spectrum of supernova remnant (SNR) G106.3+2.7 above 40 TeV, indicating that SNR G106.3+2.7 is a promising PeVatron candidate. However, the origin of the gamma-ray spectrum is still debated. Thus, a dedicated theoretical model with self-consistent descriptions is required to decipher the properties of the gamma-ray spectrum for this specific source.

Aims. We construct a theoretical model to explain the multiband photon emission from the PeVatron SNR G106.3+2.7.

Methods. In our model, the acceleration and propagation of particles from the Bohm-like diffusion region inside the SNR to the Galactic diffusion region outside the SNR are described through nonlinear diffusive shock acceleration (NLDSA). The main content of our NLDSA model is solving the hydrodynamic equations numerically for gas density, gas velocity, and gas pressure and the equation for the quasi-isotropic particle momentum distribution. The consequent multiband nonthermal emission stems from two different regions, namely the acceleration region and the escaping region.

Results. Our model is capable of explaining the multiband photon emission via the dominant synchrotron radiation of the electrons accelerated inside the SNR. The photons with energy of \geq GeV are naturally produced by the protons inside and outside the SNR. Moreover, photons in the energy range of $\sim 1 - \sim 100$ TeV are due to the interaction of escaped protons with dense molecular clouds.

Conclusions. For photons with energy $E_\gamma \geq 1$ GeV from SNR G106.3+2.7, our results here favor a hadronic origin, where the photons in the energy range of ~ 1 GeV to ~ 1 TeV are produced inside the SNR through proton-proton interaction, while photons with $E_\gamma \geq 1$ TeV originate from the interaction of escaped protons with a dense molecular cloud.

Key words. ISM: Supernova remnants – Radiative processes: Non-thermal – Gamma-rays: General

1. Introduction

Although particles in supernova remnants (SNRs) can be efficiently accelerated up to about PeV energy through the diffusive shock acceleration (DSA) mechanism (Ptuskin et al. 2010), no direct observational evidence for the acceleration of PeV Galactic cosmic rays in SNRs has been reported so far. As cosmic rays (CR) are deflected by Galactic magnetic fields, it is difficult for us to trace their sources. However, GeV-TeV gamma-ray emission can be produced through relativistic protons interacting with gas and/or a molecular cloud (MC) near the SNRs (e.g., Aharonian 2001; Gabici et al. 2007; Ohira et al. 2011). At least two SNRs (IC 443 and W 44) appear to have the characteristic pion bump feature in the gamma-ray spectra (Ackermann et al. 2013), helping us to understand the particle acceleration mechanism.

A large number of SNRs have been detected in the gamma-ray band, but none of these SNRs has been shown to emit gamma-rays to hundreds of TeV, that is, a PeV particle accelerator (or PeVatron) has not yet been confirmed experimentally. Re-

cently, HAWC, AS γ , and LHAASO experiments¹ have reported a gamma-ray spectrum of SNR G106.3+2.7 above 40 TeV, indicating that SNR G106.3+2.7 is a promising PeVatron candidate (Albert et al. 2020; Cao et al. 2021). Observation of gamma-ray emission from SNR G106.3+2.7 above 10 TeV, even up to a few 100 TeV, has also been reported (Amenomori et al. 2021), indicating that the very high-energy (VHE) gamma-ray emission above 10 TeV is well correlated with an MC rather than with the pulsar PSR J2229+6114. This morphological feature favors a hadronic origin of the VHE emission.

Recently, Xin et al. (2019) argued that the pure leptonic model for the γ -ray emission can be ruled out based on the X-ray and TeV data from SNR G106.3+2.7. According to the current understanding of acceleration and escaping processes, Bao & Chen (2021) explored a new scenario to explain the γ -ray spectrum for this source. They considered the hadronic γ -ray spectrum dominating the emission above 10 TeV to be due to the accelerated protons escaping and interacting with MCs.

¹ HAWC: The High-Altitude Water Cherenkov Gamma-Ray Observatory. AS γ : Tibet air shower experiment. LHAASO: Large High Altitude Air Shower Observatory.

The CR particles in SNRs can be accelerated through the DSA mechanism (e.g., Kang & Jones 2006; Caprioli et al. 2008; Zirakashvili & Ptuskin 2012; Telezhinsky et al. 2012a; Ferrand et al. 2014). They escape from SNRs at the so-called free escape boundary (e.g., Ellison & Bykov 2011; Telezhinsky et al. 2012b; Kang et al. 2013).

In this paper, a theoretical model is developed to explain the multiband emission from SNR G106.3+2.7, in particular, GeV to ~ 100 TeV emission. In our model, the particles are accelerated inside an SNR through DSA with Bohm-like type diffusion. Then the accelerated particles propagate outward into a different region with Galactic diffusion outside the free escape boundary. These escaped particles can produce ≥ 100 TeV photons through π^0 decay when they encounter dense MCs. Therefore, the multiband emission from the SNR G106.3+2.7 can be consistently reproduced.

2. Modeling multiband emission from SNR G106.3+2.7

2.1. Basic properties of observed multiband emission

Supernova remnant G106.3+2.7 has been observed at radio, X-ray, and γ -ray bands. Its basic features are as follows: (i) At the radio band, a brighter head and an extended tail region are evident. The overall spectral index is ~ 0.57 , and the tail region has a slightly steeper spectrum than that in the head region (Pineault & Joncas 2000). (ii) At the X-ray band, the observational data of Suzaku targeting the SNR and adjacent pulsar PSR J2229+6114 indicate that the diffusive X-ray emission is nonthermal and originates from leptonic synchrotron emission with a photon index of ~ 2.2 (Fujita et al. 2021). (iii) At the γ -ray band, a detailed analysis of GeV emission near VER J2227+608 with ten years of Fermi-LAT Pass 8 data was performed (Xin et al. 2019). Significant TeV γ -ray emission from the elongated radio extension of SNR G106.3+2.7 was detected by VERITAS (Acciari et al. 2009). In this region, emission with tens of TeV was also detected by Milagro (Abdo et al. 2007, 2009). Multi-TeV emission coincident with G106.3+2.7 has also been detected by HAWC, and the joint VERITAS-HAWC spectrum is well fitted by a power law from 900 GeV to 180 TeV (Albert et al. 2020). Recently, ≥ 100 TeV photons from the direction of SNR G106.3+2.7 were detected by AS $_{\gamma}$ experiment and LHAASO (Amenomori et al. 2021; Cao et al. 2021). Observationally, the spectral energy distribution between ~ 1 GeV and ~ 10 TeV at first appears as an increasing trend, then decreases sharply, extending to ≥ 100 TeV. Therefore, SNR G106.3+2.7 is a new potential Galactic PeVatron.

The age of SNR G106.3+2.7 still remains uncertain, with several speculations: ~ 1 kyr (Albert et al. 2020; Bao & Chen 2021), or about 10^4 yr in comparison with the characteristic age of PSR J2229+6114. Here we adopt an age of 2000 yr to match the radius (~ 5.7 pc at a distance of 800 pc) of the SNR evolution with reasonable parameters (the explosion energy $E_{\text{sn}} = 10^{50}$ erg and ejecta mass $M_{\text{ej}} = 1.4M_{\odot}$). With the adiabatic model of Kothes et al. (2001) ($n_0 = 1.9 \times 10^{24} R_f^{-5} t^2 E_{\text{sn}}$, and R_f is the shock radius), the ambient medium number density is estimated as $n_0 \sim 0.2 \text{ cm}^{-3}$.

2.2. Modeling and results

As mentioned in §1, we assumed that the multiband nonthermal emission stems from two different regions, namely the acceleration region and the escaping region. These two regions, separated

by the free escape boundary R_{esc} , retain different diffusion coefficients. Inside the radius of R_{esc} , the actual diffusion resembles a Bohm-like type, while outside the radius, Galactic diffusion dominates. For this purpose, the numerical nonlinear diffusive shock acceleration (NLDSA) model developed in Zirakashvili & Ptuskin (2012) (hereafter ZP2012 model) was adopted, as it could naturally extend from the Bohm-like diffusion region to the Galactic diffusion region (Yang et al. 2015; Tang et al. 2015).

The main content of our NLDSA model is solving the hydrodynamic equations numerically for gas density $\rho(r, t)$, gas velocity $u(r, t)$, and gas pressure $P_g(r, t)$ and the equation for the quasi-isotropic particle momentum distribution $N(r, t, p)$ (see Equations (1)-(4) of ZP2012). We extended the ZP2012 model to the Galactic diffusion region and explained TeV emission from two TeV sources in our previous work (Tang et al. 2015).

In the acceleration region, the magnetic field above the radius R_c of the contact discontinuity (CD) is given by ZP2012, and the pressure and energy flux of the magnetic field are introduced in the dynamical equation (Zirakashvili et al. 2014). In the ZP2012 model, the coordinate dependences of the magnetic field are shown as follows:

$$B(r, t) = B_0 \frac{\rho}{\rho_0} \sqrt{\frac{R_f^2}{M_A^2 V_{A0}^2} + 1}, r > R_c, \quad (1)$$

where ρ_0 and $V_{A0} = B_0 / \sqrt{4\pi\rho_0}$ are the gas density and the Alfvén velocity of the circumstellar medium; M_A determines the value of the magnetic field amplification, and for young SNRs M_A , it is about 23 (ZP2012); R_f is the radius of the forward shock (FS). However, in the region of $\leq R_c$, the magnetic field is

$$B(r, t) = \sqrt{4\pi\rho_m} \frac{|R_b - u(r_m)|}{M_A} \begin{cases} 1, & r < r_m, \\ \frac{\rho}{\rho_m}, & r_m < r < R_b, \\ \frac{\rho(R_b+0)}{\rho_m}, & R_b < r < R_c. \end{cases} \quad (2)$$

Here $r_m < R_b$ is the radius where the ejecta density has a minimum and equals ρ_m . The particle diffusion in the acceleration region is assumed to be a Bohm-like type, and the diffusion coefficient is given by $D = \eta_B D_B$, where $\eta_B = 2$ represents the possible deviations of diffusion coefficient from the typical Bohm value in a high-velocity shock, $D_B = vpc/3qB$ is the Bohm diffusion coefficient (also see ZP2012 for details).

In the escaping region, the magnetic field is assumed to be the classical Galactic magnetic field, and the diffusion coefficient can be expressed as

$$D_g(E_p) = 10^{28} \chi \left(\frac{E_p}{10 \text{ GeV}} \right)^{0.5} \text{ cm}^2 \text{ s}^{-1}, \quad (3)$$

where E_p is the accelerated proton energy, and the modification factor of $\chi = 10^{-3}$ is for slow diffusion and is much lower than that of the averaged Galactic diffusion ($\chi \sim 1$), which indicates that the diffusion is suppressed by a factor of 100 or more near SNRs (Fujita et al. 2009). According to $l = 2\sqrt{tD_g(E_p)}$ (Atoyan et al. 1995), we have $l \sim 5$ pc for a 100 TeV in a diffusing particle of 2000 yr. The escaped particles with a few hundred TeV remain in the interacting region with the nearby MC.

In our calculations, the SNR shock propagates in the ambient medium with an average hydrogen number density of $n_0 = 0.2 \text{ cm}^{-3}$, a magnetic field strength of $B_0 = 5 \mu\text{G}$, a temperature of $T = 10^4$ K, an index of the ejecta velocity distribution of

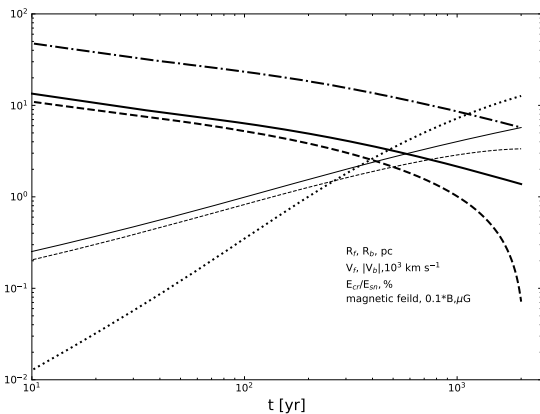


Fig. 1: Dependences on time of the forward-shock radius R_f (thin solid line), the reverse-shock radius R_b (thin dashed line), the forward-shock velocity V_f (thick solid line), the reverse-shock velocity $|V_b|$ (thick dashed line), the ratio of CR energy and energy of supernova explosion E_{cr}/E_{sn} (thick dotted line), and the magnetic field strength (thick dash-dotted line) in the shock radius ($r = R_f$).

$k = 7$, and an initial forward-shock velocity of $2.9 \times 10^4 \text{ km s}^{-1}$. The injection efficiency of thermal protons and electrons is assumed to be $\eta_f = \eta_b = 10^{-4}$ and $\eta_f = \eta_b = 10^{-7}$ at FS (f) and RS (b), respectively.

In this case, the changes in shock radii R_f and R_b , the forward- and reverse-shock velocities V_f and V_b , and the ratio of CR energy to SN explosion energy (E_{cr}/E_{sn}) with time are shown in Fig. 1. The calculations were performed until $t = 2000 \text{ yr}$, when the value of the forward-shock velocity drops down to $V_f = 1384 \text{ km s}^{-1}$ and the forward-shock radius is $R_f = 5.70 \text{ pc}$. At the Sedov stage, the reverse-shock velocity quickly decreases to 78 km s^{-1} after ~ 1000 years. Moreover, at 2000 yr , $E_{cr}/E_{sn} \approx 12\%$, approaching $E_{cr} \sim 10^{49} \text{ erg}$. Considering the gas density $n_0 = 0.2 \text{ cm}^{-3}$, the total CR energy is $\sim 3.0 \times 10^{49} (n_0/0.2 \text{ cm}^{-3})^{-1}$, which can reproduce the $\sim \text{GeV}$ gamma-ray observation (Xin et al. 2019) for this source.

The profiles of the gas, CR pressure, and magnetic pressure at the radial distance at 2000 years are shown in the top panel of Fig. 2, where the value of CR pressure is much lower than that of the gas pressure at the forward-shock position. The spatially integrated spectrum of accelerated protons and electrons is shown in the bottom panel of Fig. 2. On the one hand, because of the severe synchrotron losses in strong magnetic field, the spectrum of the accelerated electrons appears to have an obvious break. They are cut off at a few TeV. On the other hand, the proton spectrum can be approximated as a power law with a spectral index of ~ 2 below a break energy E_{cut} , and it decreases exponentially above E_{cut} . The protons inside the SNR can be accelerated up to $\sim \text{PeV}$, and the escaped protons mainly stem from the high-energy region with energy between $\sim E_{cut}$ to E_{max} (see the dashed line in the bottom panel of Fig. 2).

For the maximum energy E_{max} of the accelerated protons, a simple estimate is as follows. Because of the free-escape boundary at the $R_{esc} = \xi R_f$, maximum energy particles with distances greater than R_{esc} cannot diffuse back to the shock, and then the instantaneous maximum energy can be estimated by using $D(p_{max})/V_f = (\xi - 1)R_f$ (e.g., Caprioli et al. 2010; Morlino & Caprioli 2012), where $D(p)$ is the diffusion coefficient.

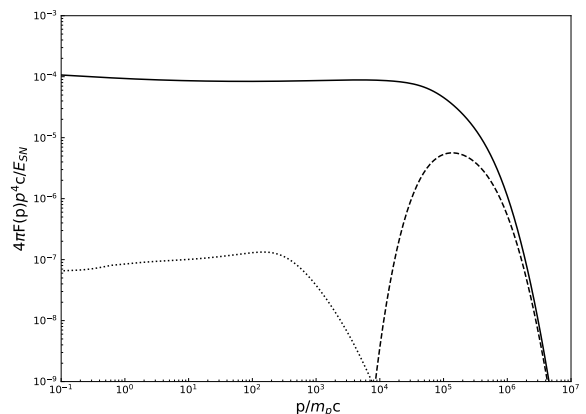
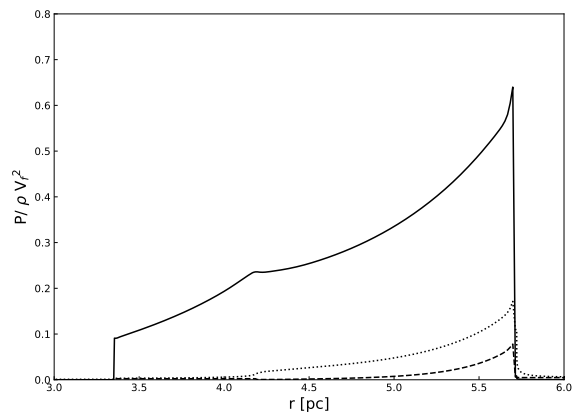


Fig. 2: Radial profiles of relevant physical quantities and spectra of particles produced in SNR. Top panel: Radial dependence of the gas pressure (solid line), the CR pressure (dotted line), and the magnetic field pressure (dashed line) at the epoch of $t = 2000 \text{ yr}$. Bottom panel: Spectra of particles produced in the whole SNR (space integrating) at the epoch of $t = 2000 \text{ yr}$. The spectra of protons include the intrinsic proton spectrum (solid line) and the electron spectrum (dotted line) inside the SNR, and escaped spectra (dashed line) integrated from $R_{esc} = 1.2R_f$ to $R_{esc,out} = 10 \text{ pc}$.

Here $\xi = 1.2$ is used, which corresponds to a diffusing distance of $0.2R_f$ upstream of the shock. The maximum energy for the Bohm-like diffusion is then approximated as

$$E_{max} = 10.4 \left(\frac{R_f}{\text{pc}} \right) \left(\frac{V_f}{1000 \text{ km s}^{-1}} \right) \left(\frac{B}{\mu\text{G}} \right) \text{ TeV}. \quad (4)$$

At the age of 2000 yr in our calculations, $R_f \sim 5.7 \text{ pc}$ and $V_f \sim 1384 \text{ km s}^{-1}$, and for the instantaneous maximum magnetic field $B \sim 50 \mu\text{G}$ in the FS upstream, the estimated $E_{max} \sim 2 \text{ PeV}$. The magnetic field strength would fall back to the background magnetic field ($5 \mu\text{G}$) as it is away from the immediate shock front (see the top panel of Fig. 2). Therefore, the value of E_{max} estimated in Eq. 4 is an upper limit. On the other hand, the value of E_{max} can be roughly estimated as follows. Because the escape particles consist of those with maximum energies in different shock positions, their spectrum has a Gauss-like distribution, as shown in Fig. 2. If $N_{esc}(p_{peak})$ represents the peak number density of the escape particles with p_{peak} , then we can

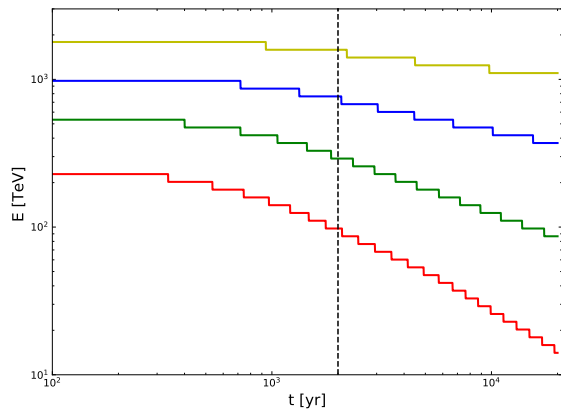


Fig. 3: Change of the energy E of accelerated particles with time for $f = 1$ (red line), $f = 0.5$ (green line), $f = 0.1$ (blue line), and $f = 0.01$ (yellow line). The definition of f is described in text.

define a parameter $f = N_{\text{esc}}(p \geq p_{\text{peak}})/N_{\text{esc}}(p_{\text{peak}})$. For a given value of f , the change in corresponding p with time can be calculated. The results for $f = 1, 0.5, 0.1$, and 0.01 are shown in Fig.3, and the maximum energy $E_{\text{max}} = p_{\text{max}}c$ can reach \sim PeV when $f \approx 0.01$. Therefore, the maximum energy of accelerated particles is $\sim 1 - \sim 2$ PeV. The values of the resulting step shape are only approximate because the momentum grid numbers are far lower than the time steps in our calculations.

In our calculations, a low injection efficiency ($\eta_f = \eta_b = 10^{-4}$) is adopted to reproduce the radio and GeV observation. If the injection efficiency for protons is high (e.g., $\eta_f = \eta_b = 10^{-2}$), then the $E_{\text{cr}}/E_{\text{sn}}$ can be approximately 70% after 1000 yr in ZP2012, and the total energy of the accelerated protons would be close to the energy of a supernova explosion. This high ratio ($E_{\text{cr}}/E_{\text{sn}} \sim 70\%$) is higher than our result here ($E_{\text{cr}}/E_{\text{sn}} = 10\%$). As a consequence, the produced GeV flux would exceed the observed flux for this source.

To characterize the regions in which the escaped protons interact with the MC in the shell with a solid angle of Ω and a radius from R_{esc} to $R_{\text{esc,out}}$ (the accelerated CR particles begin to run away from SNRs at the boundary ($R_{\text{esc}} = \xi R_f$)), we set the value of $R_{\text{esc,out}}$ as 10 pc to match the high-energy gamma ray observation. We introduced a parameter of $n_{\text{cloud}}\Omega/4\pi = 50\text{cm}^{-3}$ to describe the number density of the MC, where the n_{cloud} is the number density of the MC. It is worth mentioning that n_{cloud} cannot be determined separately because of the relation to the size of radiation region (e.g., $\Omega = \pi/3$, $n_{\text{cloud}} \sim 1500\text{cm}^{-3}$; $\Omega = 4\pi$, $n_{\text{cloud}} \sim 50\text{cm}^{-3}$). In addition, its typical density is about 100cm^{-3} , wherein the cloud could host clumps with a density of $10^3 - 10^4\text{cm}^{-3}$ (Owen et al. 2021). The total mass of the MC in the interacting region is $\sim \frac{5 \times 10^4}{\Omega} M_{\odot}$ by integrating the density from $1.2R_{\text{esc}}$ to 10 pc.

The particle (both the leptonic and hadronic) acceleration can be calculated by coupling hydrodynamic process and the evolution of the magnetic field (including the feedback between the magnetic field and the accelerated protons) inside the SNR, as well as the extension to the escaped particle diffusion outside the SNR (Tang et al. 2015). For a given SNR, the spectra of accelerated particles and escaped particles can therefore be calculated naturally at any time t . Generally, the radio and X-ray photons originate from the leptonic synchrotron emission, and the high-energy gamma-rays are produced by the proton-proton

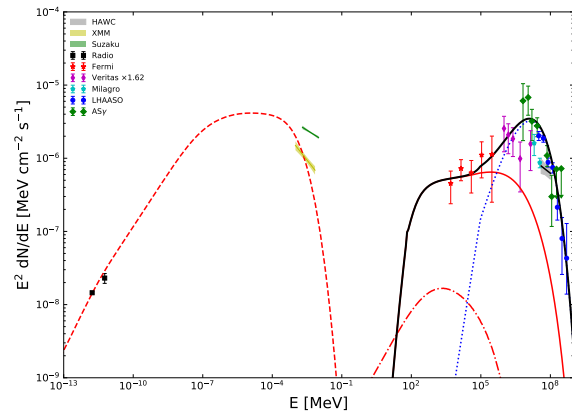


Fig. 4: Multiwave band spectra of G106.3+2.7. The red line shows synchrotron (dashed line), inverse Compton (dot-dashed line), and pp interaction (solid line) inside the SNR. The dotted blue line represents the high-energy emission from the escaped protons interacting with the MC, and the black line shows the overall VHE emission (pp interaction). Radio data of the tail region are from Pineault & Joncas (2000). The statistical uncertainties of the tail region of XMM-Newton are from Ge et al. (2020), and of the whole region of Suzaku, they are from Fujita et al. (2021). The Fermi-LAT data are from Xin et al. (2019), the VERITAS data are from Acciari et al. (2009), the Milagro data are from Abdo et al. (2007, 2009), the statistical uncertainties of HAWC are from Albert et al. (2020), the ASy data are from Amenomori et al. (2021), and the LHAASO data are from Cao et al. (2021).

interaction process (hadronic scenario) or the inverse-Compton (IC) process (leptonic scenario). Here the seed photons consist of 2.7 K microwave background light with an energy density of 0.25eVcm^{-3} , and a 25 K far-infrared radiation field with an energy density of 0.2eVcm^{-3} . Specifically, we used the emissivity formula developed by Blumenthal & Gould (1970) for the leptonic component, while the proton-proton (pp) interaction process can be calculated by analytic approximation of Kelner et al. (2006), where the hadronic scenario contains the intrinsic emission inside an SNR and the emission from its escaped protons colliding with a nearby MC.

The calculated spectral energy distribution (SED) of G106.3+2.7 with an estimated age of 2000 yr is shown in Fig. 4. From radio to X-ray band, the photons are produced through the synchrotron emission of energetic electrons in the magnetic field with a strength of $\sim 50\mu\text{G}$ at the FS position (also see the evolution of magnetic field of Fig 1). Thus, the resulting IC flux is very low due to severe radiative cooling in the strong magnetic field. Xin et al. (2019) also argued that the radio flux gives a magnetic field strength of $\sim 50\mu\text{G}$ and a corresponding $E_{\text{cut}} \sim \text{TeV}$ of the accelerated electrons in a hadronic scenario. The gamma-ray emission mainly originates from the hadronic component, and the Fermi data can be fit by the accelerated protons inside the SNR together with the escaped protons outside the SNR interacting with the nearby MC. A clearer picture is presented in Fig.5. Our results indicate that the spectrum of high-energy gamma-rays is dominated by the hadronic component, and the overall gamma-ray flux can naturally be explained by our model.

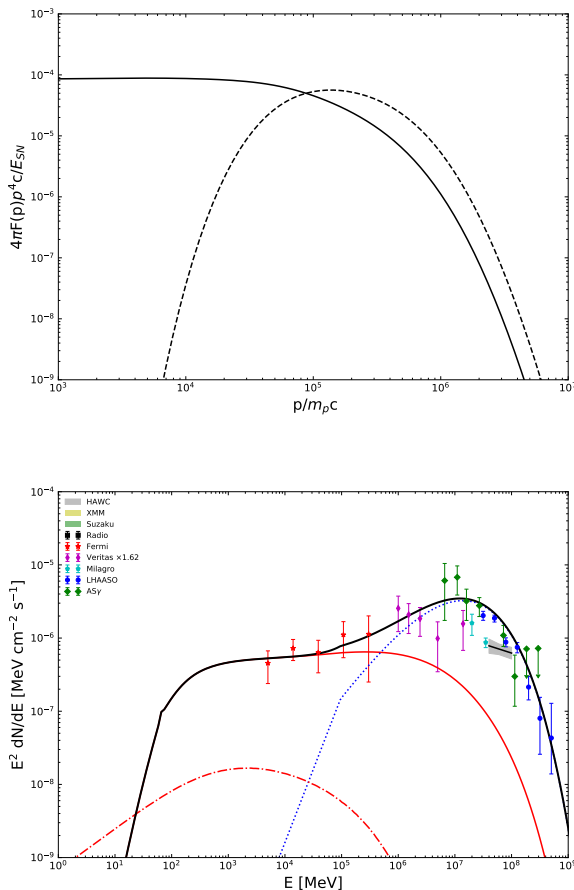


Fig. 5: Spectra of particles produced in SNR G106.3+2.7 as well as the multiwave band spectra. Top panel: Same as the bottom panel of Fig.2, but the value of the escape particle spectra is magnified by an order of magnitude. Bottom panel: Same as Fig.4.

3. Summary and discussion

The multiband photon emission from SNR G106.3+2.7 (a potential Galactic PeVatron) was studied here. The results show that photons with energy of $E_\gamma \gtrsim 1$ GeV favor a hadronic origin, where the photons in the energy range of ~ 1 GeV to ~ 1 TeV are produced inside the SNR through proton-proton interaction, and photons with $E_\gamma \gtrsim 1$ TeV originate from the interaction of escaped protons with a dense molecular cloud.

In our model, the magnetic field plays a dynamical role. Magnetic pressure and magnetic energy flux are taken into account in the shock. The amplified effects and the spatial distribution of the magnetic field were assumed using a simple parameterized description in the following. The parameter M_A and the plasma density determine the value of the amplified magnetic field strength for $r > R_c$ (see Eq. 1). In the vicinity of the CD, the plasma flow is strongly influenced by the Rayleigh-Taylor instability and results in the generation of magnetohydrodynamic (MHD) turbulence in this region. Eq. 2 is assumed to describe the amplification of the downstream magnetic field of the reverse shock. However, one important mechanism for generating an amplified magnetic field is the plasma instabilities driven by CR streaming (Bell et al. 2013; Caprioli et al. 2009), which in turn leads to a more efficient particle acceleration. In particular, the shock permeating into the dense medium is able to excite

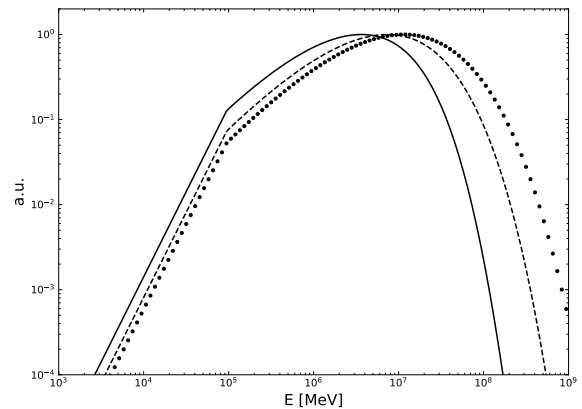


Fig. 6: Interaction of gamma-rays from the escaped protons with the same density of the MC for $\chi = 0.1$ (solid line), 0.01 (dashed line), and 0.001 (dotted line), where the gamma-ray flux maximum value is normalized to 1.

nonresonant streaming instabilities, and efficiently accelerates particles to the PeV range in the early stages (Cristofari et al. 2020a). It is noteworthy that the nonresonant growth of instabilities is expected to lead to the PeV range in only very few cases (Bell et al. 2013; Schure & Bell 2013; Cristofari et al. 2020b). For instance, based on the analysis of the nonresonant instability, Schure & Bell (2013) reported that, in the context of SNR shocks, only young SNRs in a dense environment are plausible candidates to accelerate CRs to PeV energies under some conditions (see also Cristofari et al. (2020b) for a more recent discussion). Therefore, a further investigation of MHD effects at astrophysical shocks is necessary.

In the escaping region, parameter χ of the diffusion coefficient in Eq. 3 is taken as 0.001 to fit the TeV gamma-ray spectra observed by LHAASO, which is much lower than its counterpart in the Galaxy. Near the SNR, the diffusion coefficient can be suppressed by a factor of 100 or more compared to the Galaxy (Fujita et al. 2009). In addition, we calculated the gamma-ray emission spectra for different χ values (see Fig. 6). The results indicate that the diffusion coefficient greatly affects the high-energy tail of gamma-rays.

We set the age of the SNR to 2000 yr to reproduce the high-energy data. Fig. 3 shows that the maximum energy of acceleration particles decreases rapidly at a late stage, and an older age (e.g., 10^4 yr) makes it harder to fit the high-energy data. On the other hand, the energetic escaped particles accelerated at an early stage should not reside in the interacting region with the MC.

The typical explosion energy for a thermonuclear supernova is $E_{\text{sn}} = 10^{51}$ erg. Regarding the age of SNR G106.3+2.7 (2000 yr) and the discussion in Sect. 2.1, the ambient medium number density is about 2 cm^{-3} . The total CR energy is $\sim 3.0 \times 10^{48} (n_0/2.0 \text{ cm}^{-3})^{-1}$, which leads to $E_{\text{cr}}/E_{\text{sn}} \sim 0.1\%$ for a medium number density of 2 cm^{-3} with an explosion energy $E_{\text{sn}} = 10^{51}$ erg. Therefore, the insufficient acceleration of CR protons in the shock is invoked. Everything we know about DSA suggests that young, strong SNR shocks are intrinsically much more efficient than our case here, for instance, $E_{\text{cr}}/E_{\text{sn}} \sim 10\%$. It is very difficult to produce TeV photons via DSA with this low acceleration efficiency. Hence, the explosion energy adopted

here is $E_{\text{sn}} = 10^{50}$ erg, while the estimated ambient medium number density is $n_0 \sim 0.2 \text{ cm}^{-3}$ (Kothés et al. 2001).

Here, the evolution and particle acceleration only consider type Ia SNR. However, ignoring other types is probably too simple for this specific SNR, as the actual types of the parent supernova explosion and the progenitor star are still undetermined. For type Ia SNRs, the matter distribution in the circumstellar medium (CSM) and interstellar medium (ISM) is less affected by the activities of the progenitor stars, which may result in a statistically more spherical shape. For core-collapse SNRs, however, the stellar winds blown by progenitor stars would have modified the CSM and ISM matter distribution prior to the explosion. As a consequence, the hadronic processes are affected as the matter distribution varies. A more detailed numerical simulation of particle acceleration in four types of SNRs has been conducted by Ptuskin et al. (2010). Their results indicated that the maximum energy of accelerated particles in all stages can be different for various types.

Bao & Chen (2021) have studied the hard γ -ray SED of SNR G106.3+2.7 and pointed out that the radio to X-ray band and the Fermi gamma-rays can originate from the synchrotron emission and inverse Compton of the energetic electrons, respectively. Above 10 TeV, gamma-ray emission arises from the contribution of escaped particles that interact with the MC. However, the differences between their model and our model are as follows. The acceleration and propagation of the particles are self-consistently considered through the ZP2012 model in the acceleration region with its extension (Tang et al. 2015) to escaping regions, and the hadronic contribution from two regions is predicted in our model. Moreover, the resulting IC flux with $E_\gamma \gtrsim 100$ MeV is much lower than that produced in proton-proton interaction inside the SNR because of the energetic electron cooling in a strong magnetic field.

Finally, although the gamma-ray emission can be produced via high-energy particles accelerated by the shock of the SNR G106.3+2.7 (Albert et al. 2020; Liu et al. 2020), with hadronic processes dominating the photon spectrum extending to at least 400 TeV (Xin et al. 2019; Amenomori et al. 2021), it should be pointed out that a leptonic origin of VHE γ -rays is also possible, such as in pulsar wind nebulae (Albert et al. 2020). Therefore, deeper observations are required.

Acknowledgements. This work is partially supported by National Key R & D Program of China under grant No. 2018YFA0404204, and the National Natural Science Foundation of China U1738211. C.Y. Yang is partially supported by the National Natural Science Foundation of China U2031111, U1931204, 11673060.

References

Aharonian, F. A. 2001, SSRv, 99,187
 Abdo, A. A., Allen, B., Berley, D., et al. 2007, ApJL, 664, L91
 Abdo, A. A., Allen, B. T., Aune, T., et al. 2009, ApJL, 700, L127
 Acciari, V. A., Aliu, E., Arlen, T., et al. 2009, ApJL, 703, L6
 Ackermann, M., Ajello, M., Allafort, A., et al. 2013, Sci, 339, 807
 Amenomori, M., Bao, Y.W. et al. (Tibet ASg collaboration) 2021, Nat Astron doi:10.1038/s41550-020-01294-9
 Albert, A., Alfaro, R., Alvarez, C., et al. 2020, ApJL, 896, L29
 Atoyan, A. M., Aharonian, F. A., & Völk, H. J. 1995, PhRvD, 52, 3265
 Bao, Y.W. & Chen, Y. 2021, arXiv:2103.01814
 Bell, A. R., Schure, K. M., Reville, B., et al. 2013, MNRAS, 431, 415
 Blumenthal, G. R., & Gould, R. J. 1970, RvMP, 42, 237
 Caprioli, D., Blasi, P., Amato, E., & Vietri, M. 2008, ApJL, 679, L39
 Caprioli, D., Amato, E., Blasi, P., & Vietri, M. 2009, MNRAS, 395, 895
 Caprioli, D., Amato, E., & Blasi, P., 2010, APh, 33, 307
 Cao, Z., Aharonian, F.A., An, Q. et al. ,Nature, 2021, <https://doi.org/10.1038/s41586-021-03498-z>

Cristofari, P., Renaud, M., Marcowith, A., Dwarkadas, V. V. & Tatischeff, V. 2020, MNRAS, 494,2760-2765
 Cristofari, P., Blasi, P., Amato, E. 2020, APh, 123, 102492
 Ellison, Donald C.& Bykov, Andrei M. 2011, ApJ, 731, 87
 Ferrand, Gilles, Decourchelle, Anne,& Safi-Harb, Samar 2014, ApJ, 789, 49
 Fujita, Y., Ohira, Y., Tanaka, S. J., & Takahara, F. 2009, ApJL, 707, L179
 Fujita, Y., Bamba, A., Nobukawa, K. K., et al. 2021, arXiv:2101.10329
 Ge, C., Liu, R.-Y., Niu, S., et al. 2020, arXiv:2012.11531
 Gabici, S., Aharonian, F.A. & Blasi, P. 2007, Ap&SS, 309, 365
 Kang, H., & Jones, T. W. 2006, APh, 25, 246
 Kang, Hyesung, Jones, T. W. & Edmon, Paul P. 2013, ApJ, 777, 25
 Kelner, S. R., Aharonian, F. A., & Bugayov, V. V. 2006, PhRvD, 74, 034018
 Kothés, R., Uyaniker, B., & Pineault, S. 2001, ApJ, 560,236
 Liu, S., Zeng, H., Xin, Y., et al. 2020, ApJL, 897,L34
 Morlino, G. & Caprioli, D. 2012, A&A, 538, 81
 Ohira, Y., Murase, K.& Yamazaki, R. 2011, MNRAS, 410,1577
 Owen, Ellis R. , On, Alvina Y. L., Lai, Shih-Ping, & Wu, Kinwah 2021, ApJ, 913, 52
 Pineault, S., & Joncas, G. 2000, AJ, 120, 3218
 Ptuskin, V. ,Zirakashvili, V., & Seo, E. 2010,ApJ, 718,31
 Schure, K. M., & Bell, A. R., 2013, MNRAS, 435, 1174
 Tang, Y.Y., Yang, C.Y., Zhang, L. & Wang, J. C. 2015, ApJ, 812,32
 Telezhinsky, I., Dwarkadas, V. V., & Pohl, M. 2012a, APh, 35,300
 Telezhinsky, I., Dwarkadas, V. V., & Pohl, M. 2012b, A&A, 541, 153
 Xin, Y., Zeng, H., Liu, S., et al. 2019, ApJ, 885,162
 Yang, C. Y., Zhang, L., & Wang, J. C. 2015, MNRAS, 448, 3423
 Zirakashvili, V. N., & Ptuskin, V. S. 2012, APh, 39, 12
 Zirakashvili, V. N., Aharonian, F. A., Yang, R., Oña-Wilhelmi, E., & Tuffs, R. J. 2014, ApJ, 785, 130